COMPARISON OF A COMPUTER-SIMULATED STRATUS-TOPPED BOUNDARY LAYER WITH AIRCRAFT OBSERVATIONS

SHAOHUA SHEN[1] and CHIN-HOH MOENG

National Center for Atmospheric Research,[2] Boulder, CO 80307, U.S.A.

(Received in final form 19 August, 1992)

Abstract. To assess the realism of large-eddy simulation (LES) of the stratus-topped boundary layer and its predicted turbulent structure, we performed detailed data analyses on a LES (which has a 12.5 m grid size in all three directions), in a manner similar to those used by Nicholls (1989) on aircraft measurements. The first analysis retrieves the primary convective elements, i.e., the negatively buoyant downdrafts, which are driven mainly by cloud-top radiative cooling, through a conditional sampling technique. Comparison shows that the LES of this resolution reflects most of the observed downdraft features; most of the discrepancies that exist between the obervations and the LES can be explained by decoupling of the cloud layer from the underlying flow that exists in the former but not in the latter. The second analysis shows the vertical velocity spectrum and its agreement with the measurements. In the third analysis, showing the turbulent kinetic energy budgets, the discrepancy in the turbulent transport term (i.e., the divergence of the third-moment quantity $\overline{wE}$, the turbulent-kinetic-energy flux) between the LES and measurements exists even with such a fine resolution LES. This discrepancy is related mainly to the different behavior in w^3 between the LES and observations, which may again be associated with decoupling.

An advantage of LES over aircraft observations is that the former can provide three-dimensional flow structure at any instant. In this paper, we examined the instantaneous flow structure and observed closed cellular patterns near the cloud top in which updrafts occupy the broad centers and relatively strong downdrafts occur in the narrow edges. In the intersections of these cell boundaries, there exist weak downdrafts, consisting of relatively cold and dry air, that are the most likely origins of the strong downdrafts extending throughout the mixed layer.

1. Introduction

The large-eddy simulation (LES) approach for noncloudy boundary-layer flows has been evaluated against observational data, and used extensively during the past 20 years to study the coherent structures, overall turbulence statistics, and turbulence closure problems for planetary boundary layer (PBL) parameterizations (e.g., Deardorff, 1974; Moeng and Wyngaard, 1984, 1986, 1989; Schmidt and Schumann, 1989). The basis behind the large-eddy simulation technique is that most of the turbulence eddies are explicitly calculated, thus most of the important physical processes within the clear PBL are explicitly resolved. The LES application for stratus-topped PBL, is not, however, as well-justified as for the clear PBL. In the stratus LES, many of the important physical processes (i.e., conden-

[1] Present address: Department of Physics, University of Quebec, Box 8888, Station A, Montreal, Canada H3C 3P8.

[2] The National Center for Atmospheric Research is sponsored by the National Science Foundation.

sation and radiation) have to be parameterized (Deardorff, 1980a; Moeng, 1986). The numerical simulations therefore require assessment: to what extent are the stratus LES results physically realistic?

To answer this question, it is necessary to compare LES flow in detail against measurements. So far, no detailed comparisons have been made mainly because of too coarse a resolution in the LES and the lack of observational studies of the detailed features of the stratus-topped PBL. Many observational datasets of stratus or stratocumulus have been reported, e.g., Brost *et al.* (1982a,b), Caughey *et al.* (1982), Slingo *et al.* (1982), Nicholls and Leighton (1986), and Nicholls and Turton (1986). All these studies presented results mainly of averaged statistics in which detailed flow information is lost. Recently, Nicholls (1989) presented detailed small-scale features of the convective motions within the stratus-topped PBL by conditionally sampling the same data used in Nicholls and Leighton (1986). At the same time, with the increasing power of computers, the resolution in LES has been greatly enhanced. We are now able to perform an LES with a $12.5 \times 12.5 \times 12.5$ m numerical grid mesh which makes assessment and comparison possible. As pointed out by Nicholls (1989): "Large-eddy simulations are now capable of producing details down to scales ~10 m, which are comparable with the scales measured from aircraft and will increasingly be used to study entrainment processes. It is hoped that the results presented here will be useful in assessing the realism of these simulations in a particularly difficult area for both numerical modeling and observational work".

In this study, we report a LES of the nocturnal stratus-topped PBL with a numerical resolution as fine as we can reach with current supercomputing power. The simulated flow structure is analyzed in a manner similar to that used by Nicholls (1989), and the realism of the simulated structure is assessed. It is unfortunate that the observed cases reported by Nicholls are day-time stratus clouds, while our LES is a night-time stratus case. There are certain differences (e.g., tendency of decoupling of the day-time stratus cloud layer from its subcloud layer) between the day- and night-time cases, and therefore our comparison here is meant to address only broad features. We did not compare our simulation with the stratus cloud fields observed from the Dynamics and Chemistry of Marine Stratocumulus (DYCOMS) Experiment or the First ISCCP Regional Experiment (FIRE) because we are unaware of any study that presents the detailed features of those fields.

2. The Large-Eddy Simulation Data

Our large-eddy simulation has $160 \times 160 \times 80$ grid points covering a $2 \times 2 \times 1$ km numerical domain, hence it resolves turbulent eddies down to $25 \times 25 \times 25$ m (twice the size of its grid spacing) with a numerical time step of 0.2 s. The subgrid-scale model used in the LES code is described in Moeng (1984). The geostrophic wind is 5 m/sec and the sea surface temperature is about 285 K. This simulation

TABLE I

Some statistical parameters

Cases	Simulation	Observation
w_* (m/s)	0.70	0.62
T_* (K)	0.029	0.026
Q_* (g/kg)	0.017	0.029
w_e (cm/s)	0.56	0.75
ΔT_v (K)	5.97	6.88
Δq (g/kg)	−1.56	−3.28
h (m)	470	370–1120
R (K h^{-1})	6.1	5.1–7.1

* R is the maximum cooling rate near the cloud top.

includes parameterized interactive long-wave radiative cooling and latent heating processes; those two schemes are described in Moeng (1986). It excludes solar radiation to represent the nocturnal stratus-topped PBL. After the simulation reaches a quasi-steady state, we recorded seven LES datasets, over a period of about two large-eddy-turnover times, for the following analysis. During this period, the mean cloud top height grows from 463 to 473 m. The cloud-base height is about 250 m. At the cloud top, the averaged virtual potential temperature, moisture mixing ratio, and radiative cooling rate are about 285.7 K, 6.9 g/Kg, and 6.1 K/hr, respectively. The surface buoyancy flux is positive but rather small; it is about 5 W/m^2. The surface moisture flux is about 15 W/m^2. The dominant large eddies have a horizontal width of about the depth of the cloud-top height, so the 2 km extent of our horizontal domain covers about four such eddies in each direction; this, along with time averaging over the recorded seven datasets, should be adequate in representing the large eddies.

The scaling parameters of the vertical velocity, temperature, and moisture used in this study are defined as follows:

$$w_* \equiv \left[z_i \frac{g}{T_0} (\overline{wT_v})_{\text{cld}} \right]^{1/3}, \tag{1}$$

$$T_* \equiv (\overline{wT_v})_{\text{cld}} / w_*, \tag{2}$$

$$Q_* \equiv (\overline{wq_v} + \overline{wq_l})_{\text{cld}} / w_*, \tag{3}$$

as suggested by Moeng (1986), where z_i is the mean cloud top, g/T_0 the buoyancy coefficient, T_v the virtual temperature, q_v the water vapor mixing ratio, q_l the liquid water mixing ratio, w the vertical velocity, and $(\overline{wT_v})_{\text{cld}}$ and $(\overline{wq_v} + \overline{wq_l})_{\text{cld}}$ are the layer-averaged virtual temperature and total moisture fluxes within the cloud layer. Nicholls' scaling parameters were defined in a slightly different manner. He defined Q_* using the moisture flux at the cloud-top level. Since the moisture flux profile varies in height, we believe that the use of a cloud-layer-averaged moisture flux is more representative. Table I lists the relevant statistics.

We adopted a method in computing the cloud-top jumps ΔT_v and Δq similar to that used by Nicholls (1989). They are computed as: $\Delta f = \Sigma_x \Sigma_y [f(x, y, z^+) - f(x, y, z^-)]$, where f is either T_v or q; z^+ is the level just above the highest cloud-top level (that is, $z^+ = \max[z_{\mathrm{TOP}}(x, y)] + \Delta z$, where $z_{\mathrm{TOP}}(x, y)$ are the local cloud tops and Δz is the vertical grid interval); z^- is the level just below the lowest cloud-top level.

This simulated stratus cloud has a liquid-water-moist-static-energy jump, $\Delta h_l \sim 6.7$ K and a total moisture mixing ratio jump, $\Delta q \sim -1.6$ g/Kg, which gives an equivalent-potential-temperature jump, $\Delta \theta_e \sim 2.5$; therefore, according to the criterion suggested by Randall (1980) and Deardorff (1980b), the cloud layer is stable with respect to the cloud-top entrainment instability.

Before comparing the results of LES and Nicholls' aircraft measurements, it is useful to examine the spatial structure of w', T_v', q' (total moisture mixing ratio) and q_l' fields in horizontal cross-sections at various heights at any instant. Figure 1 presents these fluctuations at $z = 0.95 z_i$. At this level, we observe closed cellular patterns in which the updrafts occupy the broad centers and strong downdrafts occupy the narrow edges. These cellular patterns are evident only when the grid mesh is as fine as this simulation. The diameter of the quasi-circular cellular pattern is about four times the width of the downdrafts. This cellular pattern near cloud top was also observed by Nicholls and Leighton (1986), among others. Nicholls (1989) found that the mean cell diameter is about four times the width of the downdraft region near cloud top, consistent with our LES results.

There are weak, broad downdrafts occupying the intersecting area among several cell boundaries, as marked by X's in Figure 1. Minima of virtual temperature, moisture, and liquid water fluctuations are likely to occur in these areas, suggesting that not only does much of the radiatively cooled air converge into these regions but also most of the dry air from the inversion is entrained (or engulfed) into these regions as well. As we shall see later from Figures 2–4, these areas are the likely origins of strong coherent downdrafts that extend down to the mixed layer.

Figures 2a–c show the vertical velocity, temperature, and total moisture fluctuations at $z = 0.5 z_i$. At this height, the closed cellular structure is no longer obvious. The dominant structures are thermal plumes in which the width of the updrafts and downdrafts are approximately the same. The negative buoyancy regions become broader and their strength decreases, in comparison with those at $z = 0.95 z_i$. Vertical velocity and virtual potential temperature are well correlated. The negative moisture fluctuations also become smaller, but they have better correlation with downdrafts than at $z = 0.95 z_i$.

At $z = 0.1 z_i$, near the surface, the flow pattern (Figure 3) shows that several relatively strong downward plumes have traveled to this height; most of them are associated with large negative T_v and q at this height. Many of the strong downward plumes which travel to this level originated from the intersections of the cell boundaries near the cloud top, marked with X's in Figure 1. This feature looks similar to the clear convective PBL reported by Clark (1979), Mason (1990), and

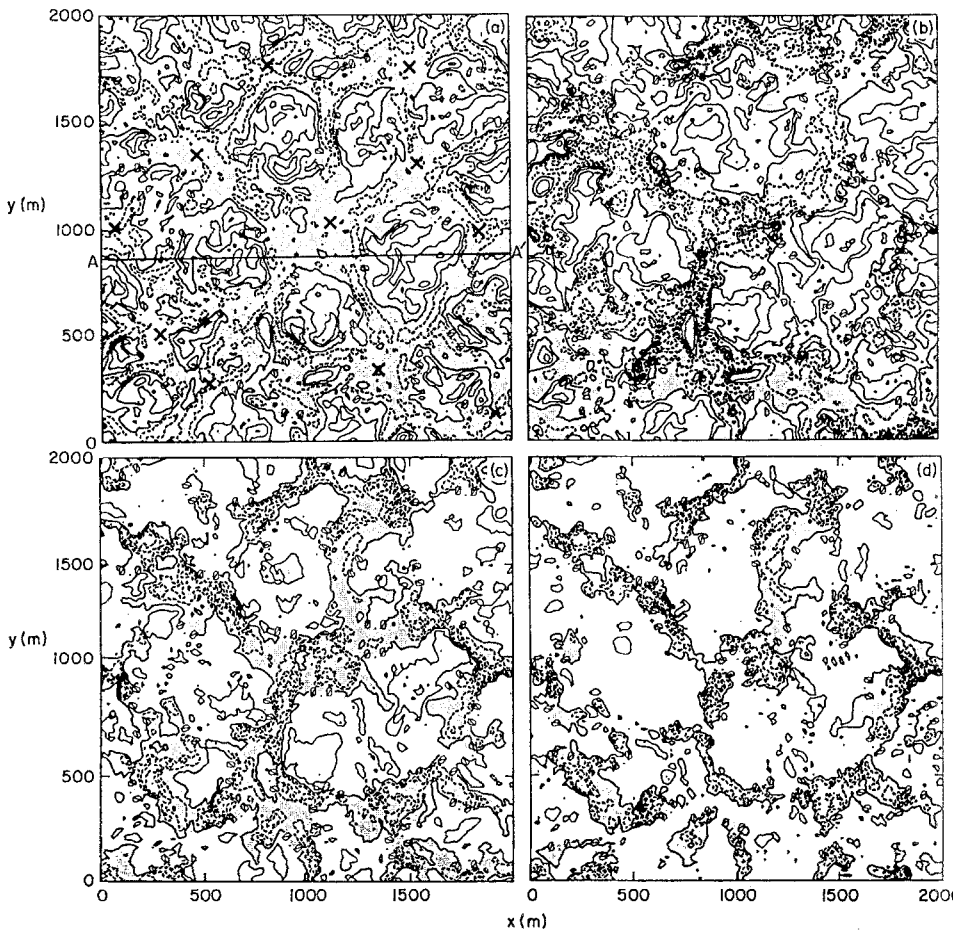

Fig. 1. Horizontal cross sections of (a) w', (b) T_v', (c) q', (d) q_l' at $z = 0.95z_i$. The solid and dashed contour lines represent positive and negative values, respectively.

others who found that clear-air upward thermals tend to originate at the intersections of the cell boundaries near the surface. However, as pointed out by Nicholls (1989) and Moeng and Schumann (1991), the dynamical origins of cloud-top-cooled downdrafts and surface-heated updrafts have a subtle difference: the surface-heated updrafts in the clear convective PBL are accelerated near the surface mainly by buoyancy, while the cloud-top-cooled downdrafts in the stratus-topped PBL are forced near the cloud top mainly by horizontal flow convergence.

Next, in Figure 4, we show a vertical cross-section of the vertical velocity, virtual temperature, moisture, and liquid water at $y = 937.5$ m (i.e., along A–A′ in Figure 1), which was selected to identify individual convective elements. It shows several downdrafts, some of which extend down throughout the whole PBL as seen in

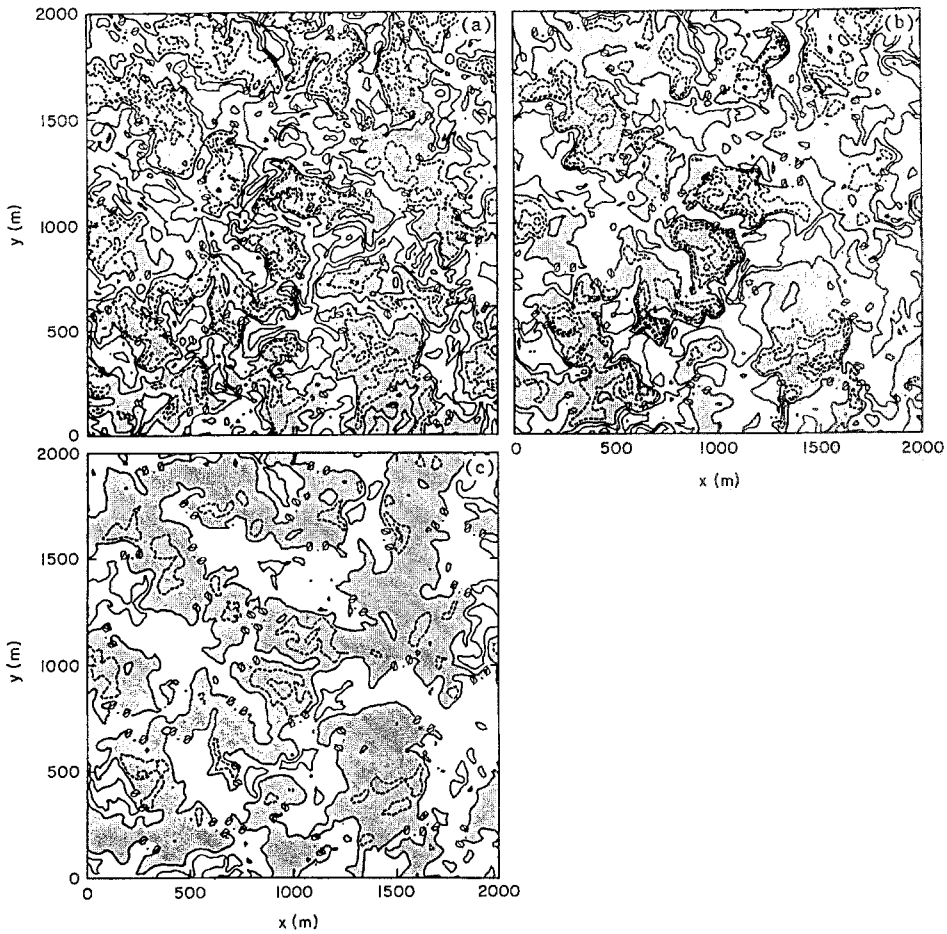

Fig. 2. Same as Figure 1, but at $z = 0.5z_i$.

Figures 4a and 4c (e.g., $x \sim 20$ m and $x \sim 1600$ m, near the surface). Local negative buoyancy maxima are located in the cloud layer.

3. Comparison with Aircraft Measurements

In the previous section, we have examined the simulated instantaneous spatial fluctuations of q, q_l, T_v, and w. To assess this LES flow field, we shall retrieve the downdraft structure of the simulated field in a method similar to that used by Nicholls (1989) for aircraft measurements and try to make as detailed a comparison as possible.

The aircraft data analyzed by Nicholls (1989) were obtained from five flights by the Meteorological Research Flight C-130 research aircraft in horizontally exten-

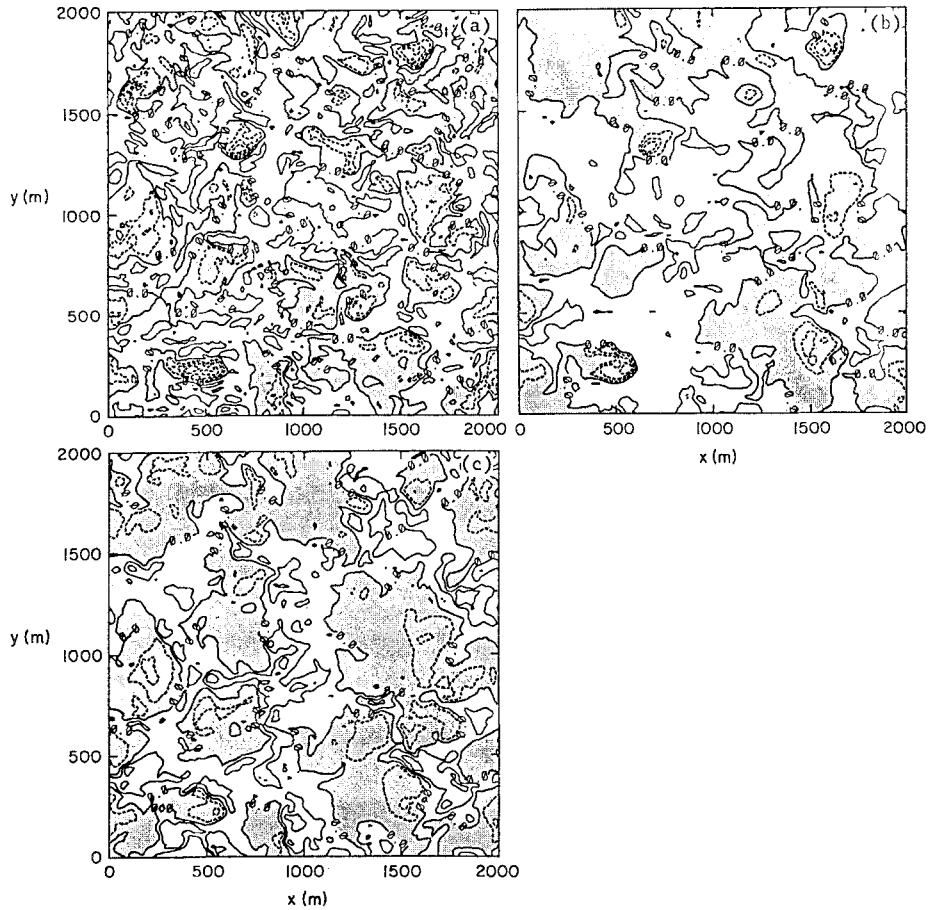

Fig. 3. Same as Figure 1, but at $z = 0.1z_i$.

sive, uniform stratiform cloud sheets over the North Sea. The cloud layer was found to be decoupled from the surface in four of the five observations (except in case 624); that is, the mixed layer is separated from the surface. Hence, Nicholls showed the results of downdraft structure only within the mixed layer instead of the whole PBL. In those cases, the convective motions within the cloud layer were driven mainly by cloud-top radiative cooling, with little heat flux input from the surface. These aircraft measurements were also studied by Nicholls (1984) and Nicholls and Leighton (1986). Some relevant statistics of observational data, averaged over five flight cases, are given in Table I.

In the following figures, we plot only the profiles below cloud top level; above cloud top, statistics depend on environmental conditions, such as inversion depth and strength. The LES results are represented by solid lines and those of Nicholls by dots. Our LES excludes solar radiation and drizzle, and has a well-mixed layer

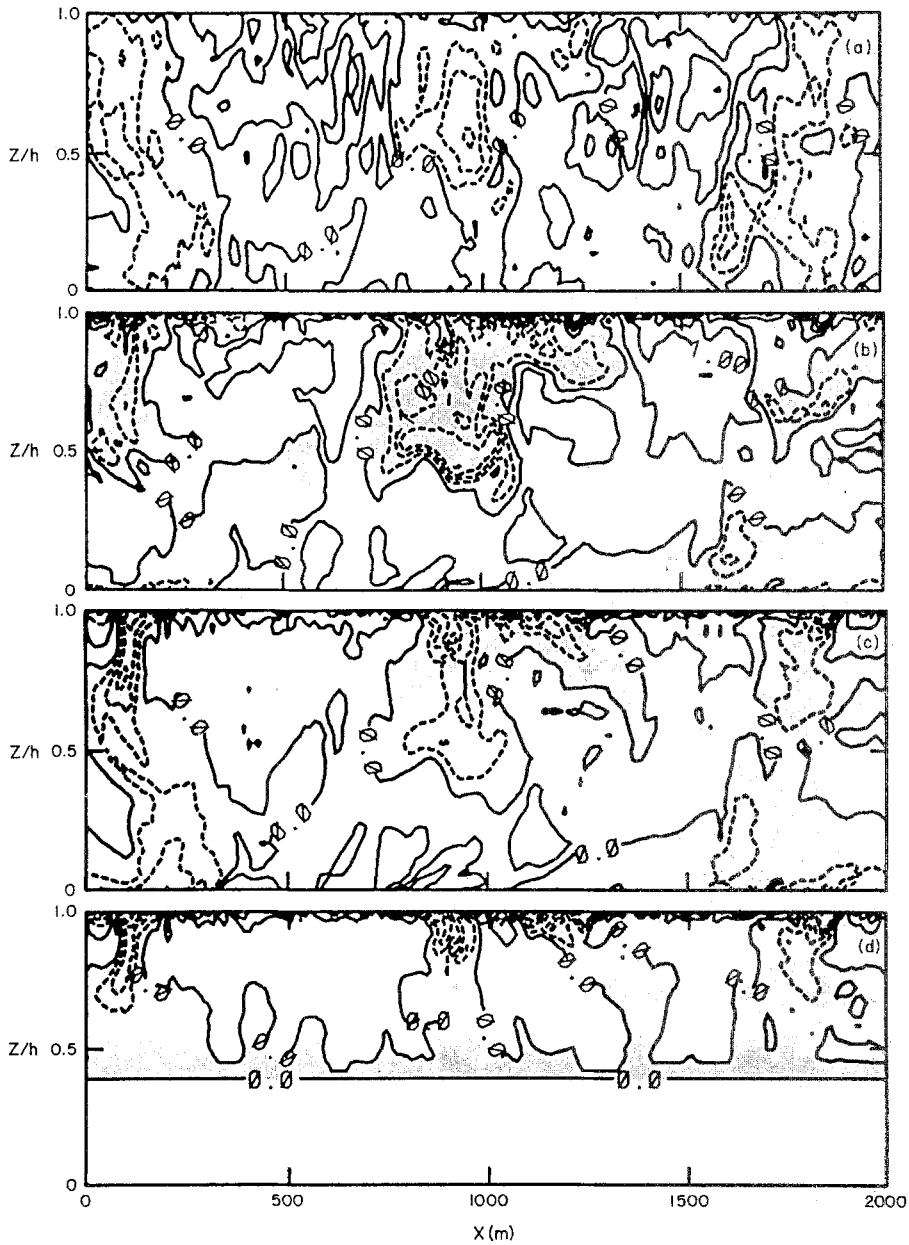

Fig. 4. Vertical cross-sections of (a) w' (b) T_v', (c) q', (d) q_l' along $A - A'$ in Figure 1. The solid and dashed lines represent positive and negative values, respectively.

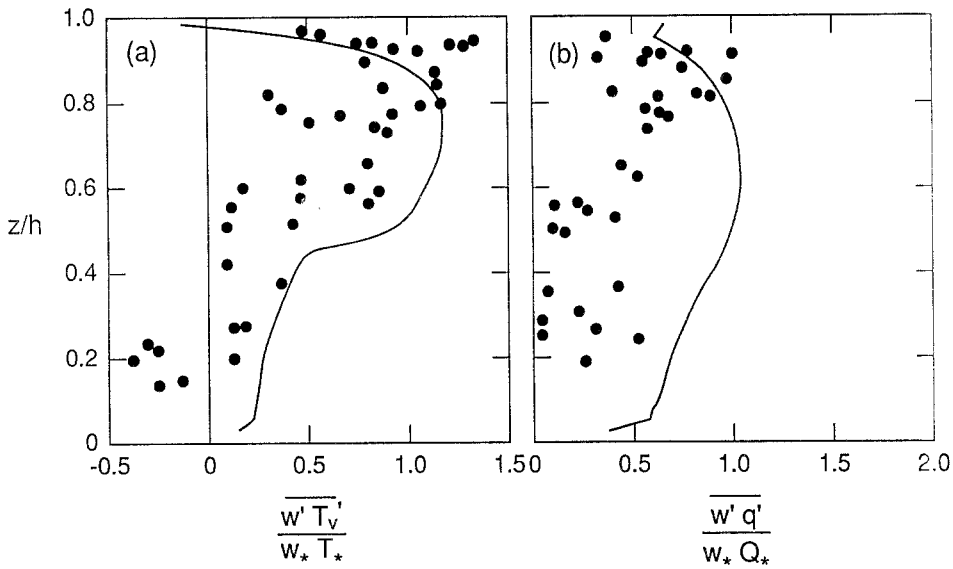

Fig. 5. Comparison of (a) buoyancy fluxes and (b) total moisture fluxes between the LES (solid lines) and the measured data (dots).

extending from the cloud top down to the surface. In the following figures, h represents mixed-layer depth. (Note that z_i represents mean-cloud-top height, which is not the same as h in Nicholls' cases.) Thus, $z/h = 0$ in the following figures indicates the surface for the LES results, while it indicates the mixed-layer base (which is the cloud base height in two of Nicholls' cases and is the surface in Flight 624) for the observational results. In both cases, $z/h = 1$ indicates cloud-top level.

3.1. Ensemble-mean statistics

To show the overall differences between the simulated and observed stratus clouds, we will first compare their ensemble-mean statistics; these statistics are represented by line averaging over an 8-min aircraft path, but by horizontal area averaging (and about two large-eddy-turnover-time averaging as well) in the LES results. As we shall see, most of the differences can be explained by the existence of a decoupled layer in the observed cases. Figure 5 shows the total buoyancy and moisture fluxes. The fluxes were scaled with the parameters defined in Equations (1)–(3). The buoyancy flux is positive within the whole mixed layer and is larger within than below cloud because of the latent heating. In Nicholls' cases, the buoyancy flux decreases sharply away from the cloud top and becomes negative near the base of the mixed layer; these sharp decreases in height and the negative buoyancy flux at the mixed-layer base are associated with decoupling.

The total moisture flux is about twice as large in the LES as in the observations.

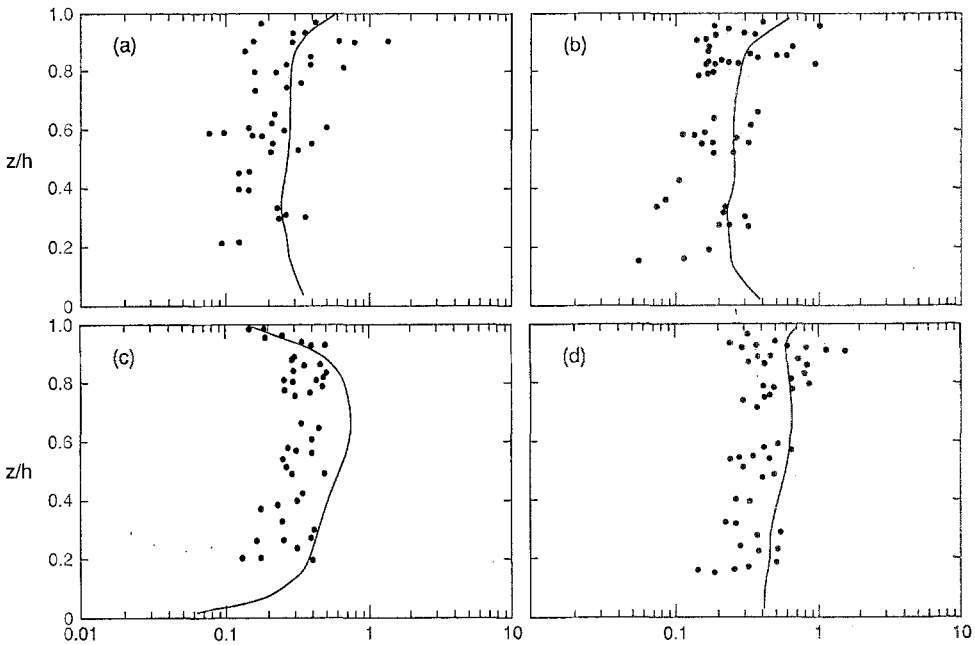

Fig. 6. Comparison of (a) u-variance, (b) v-variance, (c) w-variance, and (d) the total kinetic energy between the LES (solid lines) and the measured data (dots).

The much larger LES moisture flux is due partly to the different surface conditions; this LES represents the subtropical maritime stratus where the sea surface moisture supply is much larger than over the U.K. where Nicholls' observations were taken. In addition, most of the observed clouds were decoupled from the subcloud layer, hence there was no moisture supply from the surface. It can be clearly seen that near $z/h = 0$ (which is the sea surface in LES and the base of the mixed layer in Nicholls' data), the LES moisture flux is positive, while Nicholls' flux is nearly zero.

Figure 6 shows the scaled velocity variances and turbulent kinetic energy (TKE). The total TKE is nearly uniform in height. The vertical velocity variance increases with height from the surface and reaches a maximum at about $z = 0.8z_i$. The LES results agree with observational data in the upper part of the mixed layer, but are slightly larger in the lower part of the mixed layer. The latter is consistent with the existence of a slightly stable layer (which acts to decrease the kinetic energy) near the cloud base in the observations.

The normalized variances of temperature and total moisture are given in Figure 7. Throughout most of the mixed layer, the LES temperature and moisture variances are smaller than observations due perhaps to the unresolved-scale motions in the LES which include eddies larger than the numerical domain and eddies smaller than 25 m (twice the size of the grid mesh). The coherent downdrafts that

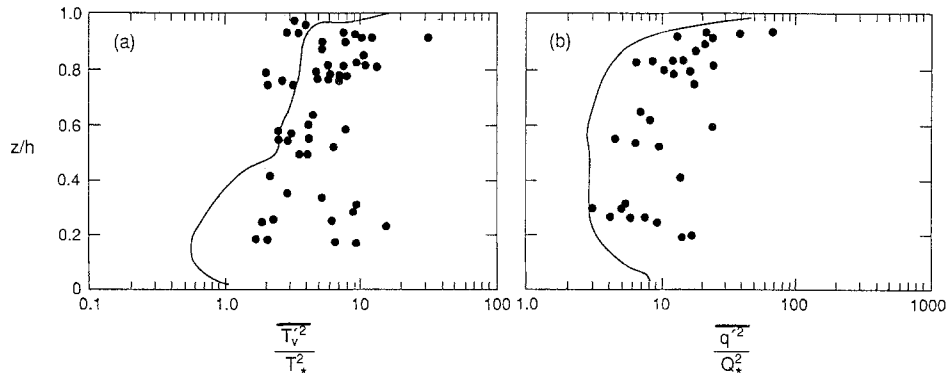

Fig. 7. Comparison of (a) temperature variance, and (b) moisture variance between the LES (solid lines) and the measured data (dots).

we shall analyze next are dominated by the eddies of the size of the mixed-layer depth, and hopefully their properties are not affected much by the above-mentioned unresolved eddies.

3.2. Conditional sampling technique

Coherent downdrafts are the most important feature for carrying turbulent fluxes in the stratus-topped PBL (Caughey *et al.*, 1982; Nicholls, 1989). Here, we apply a conditional sampling technique, similar to the one used by Nicholls for the aircraft data, to the simulated flow field. Since conditional sampling results are sensitive to the selection criteria for events (Lenschow and Stephens, 1980; Khalsa and Greenhut, 1985; Young, 1988a, b; Nicholls, 1989; Schumann and Moeng, 1991a, b), it is necessary to use a sampling technique similar to that used by Nicholls (1989) when we apply it to the LES field.

The criteria we set for a downdraft event are that w' must be less than a given threshold w_{thres} and must have a positive correlation with the vertical velocity at the mid-PBL to guarantee some degree of vertical coherence. The latter criterion was not used by Nicholls (1989); however, Nicholls mentioned that some degree of vertical coherence was ensured in his analysis. In our selection, we make the choice $w_{\text{thres}} = -0.5w_*$. We first identified all downdrafts along the x direction at all y points on each horizontal plane. We then picked up the downdrafts at grid points where $w' < w_{\text{thres}}$ and $w'w'_{\text{ref}} > 0$ (where w'_{ref} is w' at the mid-PBL). The nearest zero crossing points on either side define the extent of the event and its intersected width, d. Furthermore, we selected only downdrafts that have widths larger than $z_i/20$, as used by Nicholls.

Following Nicholls (1989), we also composited the events by interpolating the conditional sampled events (which have different horizontal sizes) to a certain normalized grid size as shown in Figure 8, in which the ten points (i.e., $\pm i = 1$ to

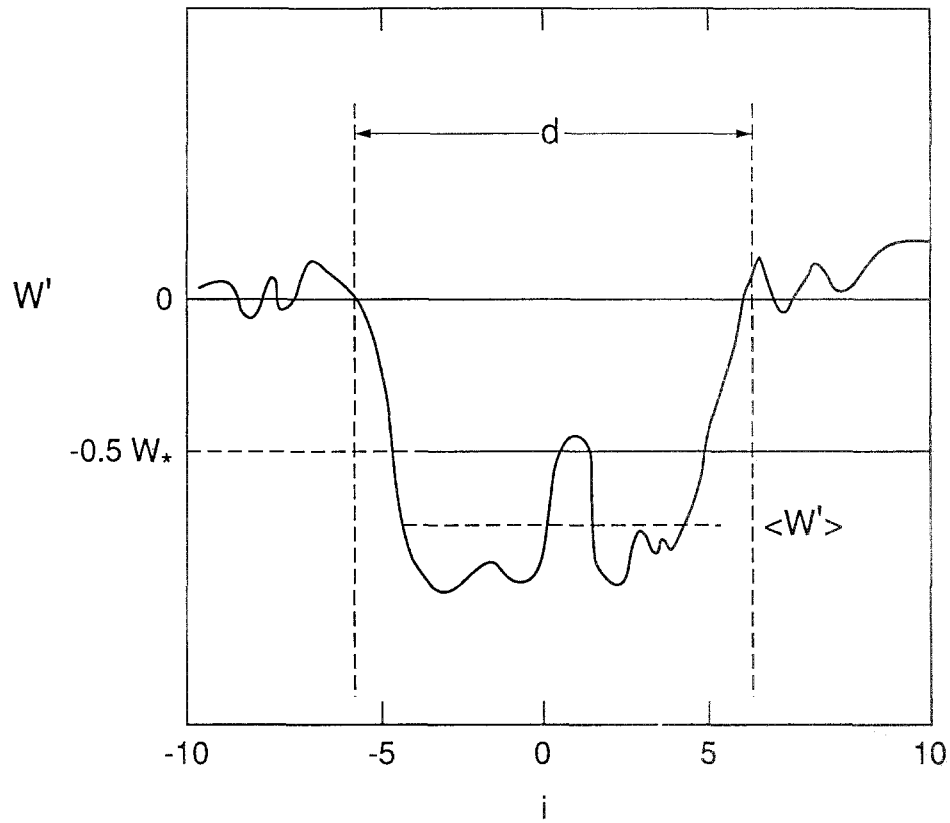

Fig. 8. A sketch that shows a typical conditionally sampled event interpolated to a certain normalized grid size.

5 in the abscissa) are within each event and another five points (i.e., $\pm i = 6$ to 10) were added to each side of the event boundaries to represent the immediate surroundings. If the 'tails' section extended into a region occupied by another selected event, we discarded that tail section as did Nicholls (1989).

If there are n events being selected on each LES horizontal plane and over the seven recorded time intervals, then the event average $\bar{f}'(z, i)$ is

$$\bar{f}'(z, i) = \sum_n f'(z, i)/n \,, \tag{4}$$

the mean intersected event width, $\bar{d}$, is

$$\bar{d} = \sum_n d/n \,, \tag{5}$$

the mean number of events per unit length h in the x direction for all y, N, is

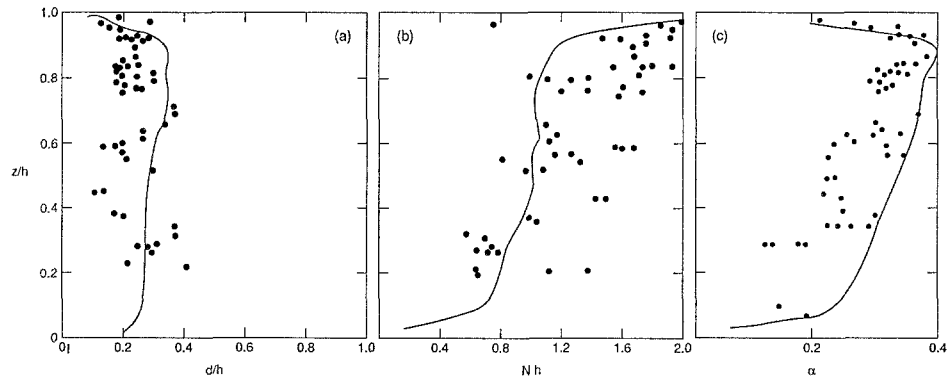

Fig. 9. Comparison of (a) $\bar{d}/h$, (b) Nh, and (c) a computed from LES (solid lines) with the measured data (dots).

$$N = \frac{1}{M_x \Delta x}\left(\frac{n}{M_y}\right), \tag{6}$$

and the fractional area occupied by events, a, is

$$a = N\bar{d}\,, \tag{7}$$

where M_x and M_y are the total grid points along the x and y directions, respectively, and Δx is the grid spacing along the x direction.

The mean value of one event $\langle f' \rangle$, excluding the two points adjacent to the boundaries as used by Nicholl's (1989), is defined as:

$$\langle f'(z) \rangle = \sum_{i=-4,+4} \bar{f}'(z, i)/8\,. \tag{8}$$

Figure 8 is a schematic diagram showing a downdraft event and the mean value associated with it. Readers are referred to Nicholls (1989) for a more detailed description.

3.3. Event means

Figure 9 shows the mean width of all events normalized by the mixed-layer depth, $\bar{d}/h$, the mean number of events, Nh, and the mean fractional area occupied by all selected events, a, from the LES and Nicholls (1989). The mean width of the LES downdrafts is about $0.3h$, while the observed is about $0.2h$. The mean width of downdrafts is rather constant in height below $0.9h$ in both LES and observations. Above $0.9h$, the LES width decreases sharply to nearly zero at the cloud-top. We note that the definition of the mean cloud top may be quite different between the LES and aircraft data analyses. In the LES, we define the mean cloud top z_i (or h) by horizontally averaging the cloud tops. It is not clear how Nicholls defined his cloud-top level from the aircraft data. The mean number of events is also

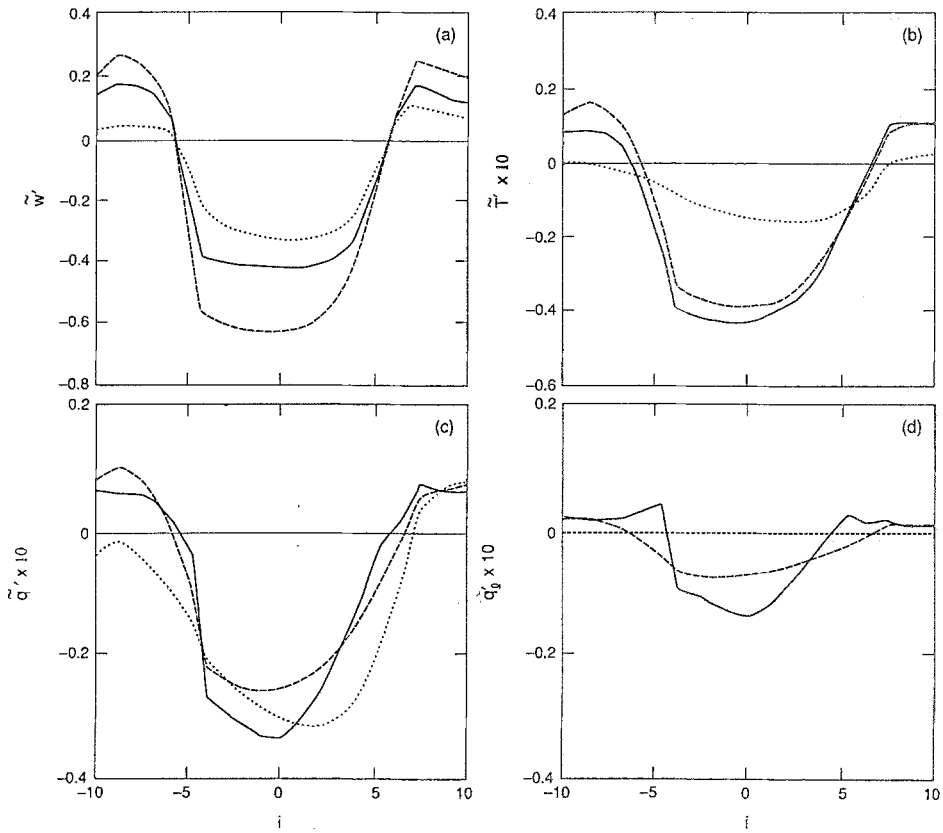

Fig. 10. Composite conditional sampling mean values of (a) vertical velocity, (b) temperature, (c) total moisture mixing ratio, and (d) liquid water mixing ratio computed from the LES at three levels: '———', 37.5 m below the cloud top, '– – –', 187 m below the cloud top, '.....', 375 m below the cloud top.

rather constant between $0.2h$ and $0.9h$, and rapidly increases above $0.9h$, where entrainment and the mixing of cloud and inversion air are active. The number of downdrafts decreases sharply near the surface. The fractional area steadily increases upward from the surface to about $0.9h$ and decreases sharply to zero above it. Overall, the LES results show general similarity with the observed results.

Figure 10 shows the horizontal distributions of vertical velocity, temperature, total water, and liquid water averaged over all selected events from the LES data. The three different curves in Figure 10 represent these distributions at three different heights: 37.5 m (solid line), 187.5 m (dashed line) and 375 m (dotted line) below the averaged cloud-top height, respectively; these levels are about the same as those selected by Nicholls (shown in Figure 11). The comparison of the solid lines between LES and observations should reveal mainly the differences of the near cloud-top processes (such as entrainment, cloud-top radiative and evaporative

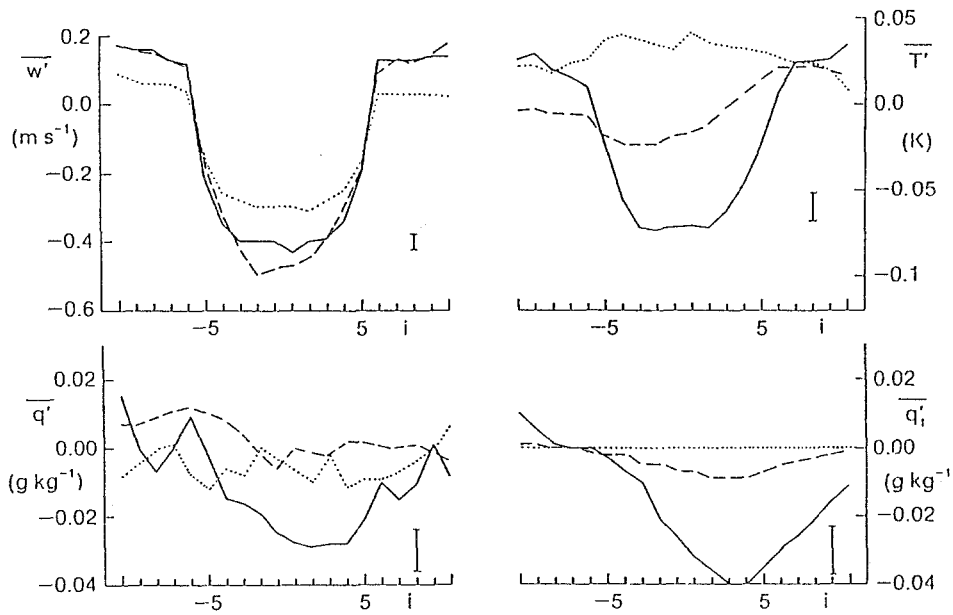

Fig. 11. Composite conditional sampling mean values of (a) vertical velocity, (b) temperature, (c) total moisture mixing ratio, and (d) liquid water mixing ratio computed from the flight 511 at three levels: '——', 40 m below the cloud top, '– – –', 180 m below the cloud top, '.....', 385 m below the cloud top. The error bars indicate the typical standard deviation of the mean of data points within the events boundaries ($-5 < i < 5$). (This figure is taken from Nicholls, 1989.)

cooling), while that of dashed and dotted lines (which represent events well into the mixed layer) may reveal differences due to other factors, e.g., internal solar absorption, drizzle, and other decoupling processes. The vertical velocity fluctuations compare well between the LES (Figure 10) and the observations (Figure 11); however, discrepancies are found in the thermal and moisture fields. The nearly top-hat distribution within events exists in all fields in LES, but is obvious only in the w-field in observations. Near the cloud top, the LES downdraft temperature fluctuations are smaller than observed. However, at 187 and 375 m below the cloud top, the LES downdraft temperature fluctuations become much larger than observed; at 375 m, the observed and the LES downdraft temperature fluctuations even have opposite signs; the slightly warmer-than-environment downdrafts at 375 m below the cloud top in the observed cases are associated with the cloud-base decoupling where the buoyancy flux becomes negative. And because of decoupling, the moisture supply from below (mostly into updrafts) shuts off; thus the moisture fluctuations within the observed composite downdraft are about zero relative to their environment. Since no decoupling exists in the LES, the downdrafts remain much drier than the updrafts (i.e., a larger magnitude of $\bar{q}'$) throughout most of the mixed layer. The comparison between the liquid water fields is fair, except the near-cloud-top level where the observed liquid water is much

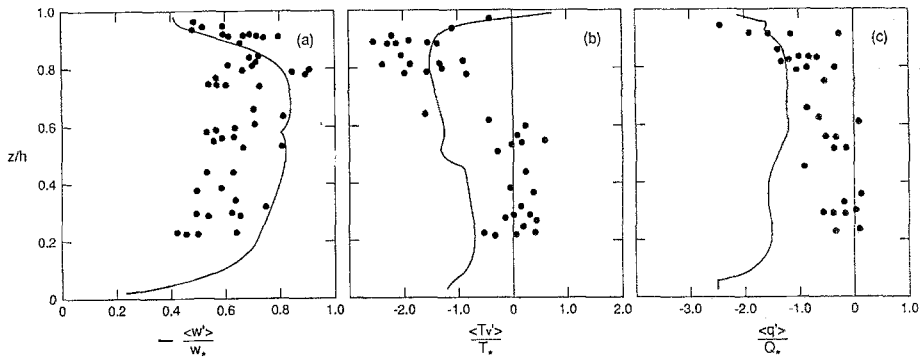

Fig. 12. Vertical distributions of the conditionally sampled means of (a) vertical velocity, (b) virtual temperature, and (c) total moisture mixing ratio from the LES (solid lines) and the measured data (dots).

larger within the downdrafts. We do not know how much of the discrepancy is due to the uncertainty of Johnson–Williams liquid-water sensor measurements and how much is due to the unresolved small-scale mixing process in the LES.

Figure 12 compares the vertical distributions of the means of all events, $\langle w' \rangle$, $\langle T_v' \rangle$, and $\langle q' \rangle$, in dimensionless forms. The profile of $\langle w' \rangle / w_*$ from the LES is similar to that observed but our magnitudes are slightly larger below $0.8h$, the level where both LES and observations show a maximum strength of the downdraft events. Large differences are found in $\langle q' \rangle$ and $\langle T_v' \rangle$ within the whole mixed layer, particularly in the lower half. The differences in the lower mixed layer are largely due to the decoupling that exists in the observations but not in the LES. Decoupling implies the existence of a slightly stable layer (i.e., a negative buoyancy flux layer) near the cloud base, hence the observed downdrafts are slightly warmer than the updrafts (i.e., $\langle T_v' \rangle$ becomes slightly positive). In addition, decoupling shuts off the moisture supply from below which goes mainly into updrafts, so the observed downdrafts (relative to updrafts) have a nearly zero moisture fluctuations near the cloud base.

3.4. Event variances

Event variances are measures of small-scale fluctuations within the events. The ratio of variance within downdrafts relative to the total variance, which Nicholls (1989) called the "effectiveness ratio", can be expressed as:

$$r(f) = \langle f'^2 \rangle / \overline{f'^2}\,, \tag{9}$$

where the bracket represents the event mean and the overbar represents the ensemble mean. This ratio measures the contribution of the selected downdrafts to the net variances. (However, since the fractional area occupied by the downdrafts is less than 0.5 as shown in Figure 9, the relative contribution of downdraft

events to the variances per unit length is actually higher than it appears in Figure 13; Nicholls (1989) discussed this effect. We shall not discuss in detail the downdraft contributions here.) Overall, our LES underestimates the w and T fluctuations within the events in the upper half of the mixed layer, which may be due to the internal solar heating in the observed clouds and the small eddies not resolved in the LES. In the lower half of the mixed layer, the $r(T)$ of the LES is much larger; this may be due to the much smaller denominator in Equation (9), i.e., the smaller $\overline{T'^2}$ in LES than in observations as shown in Figure 7. Both $r(q)$ and $r(q_l)$ from the LES are fairly consistent with the observational data.

3.5. Vertical velocity spectra

To compute the one-dimensional vertical velocity spectra along the x-direction from LES, we first Fourier transformed the vertical velocity field in each horizontal plane to wavenumber space, i.e., from $w(x, y)$ to $\hat{w}(k_x, k_y)$, and averaged the spectrum over k_y:

$$S_w(k_x) = \sum_{k_y} (R[\hat{w}(k_x, k_y)] \times R[\hat{w}(k_x, k_y)] + I[\hat{w}(k_x, k_y)] \times I[\hat{w}(k_x, k_y)]) , \tag{10}$$

where $R[\hat{w}(k_x, k_y)]$ and $I[\hat{w}(k_x, k_y)]$ are the real and imaginary parts of $\hat{w}$, respectively. The results, after being normalized by $k_x/(w_*^2 \phi_\epsilon^{2/3})$ and averaged over the seven recorded datasets, are shown in Figure 14, where $\phi_\epsilon = \epsilon z_i / w_*^3$ is the dimensionless dissipation rate. The vertical velocity spectra at $0.1h$, $0.5h$, and $0.95h$ are compared with Nicholls' spectra shown in Figure 15. The scaling that we used to normalize the vertical velocity spectra is similar to that used in Kaimal *et al.* (1976) and in Nicholls and Readings (1981), but different from that used in Nicholls (1989). The scaling method used by Nicholls (1989) is not clear to us, so we shall not compare the absolute values of these spectra. Rather, we shall compare only the distributions. The shape of our vertical velocity spectra is basically similar to that reported in Nicholls (1989). Our spectral peaks become broader with height.

In Figure 16, we plotted the vertical distributions of the peaks of the normalized spectra as h/λ_m vs. height, where λ_m is the wavelength of the spectrum peak. The bars covering the broad range of the peak spectrum found in the LES are drawn by visual inspection on the spectra shown in Figure 14. The LES and observation results compare well except in the lower part of the mixed layer where the LES spectra seem to peak at a higher wavenumber. (In the LES, the spectral peaks are located in a higher wavenumber region below $z = 0.5z_i$ than those between $0.5z_i$ and $0.8z_i$.) This difference is likely due to the lower boundary of the analysis data. The lower boundary of our mixed layer is a rigid surface that tends to produce smaller scale eddies, while $z/h = 0$ in Nicholls' cases is away from the rigid surface except in Flight 624; unfortunately, Nicholls showed no spectral data in this region for Flight 624. Our results seem to be consistent with those reported

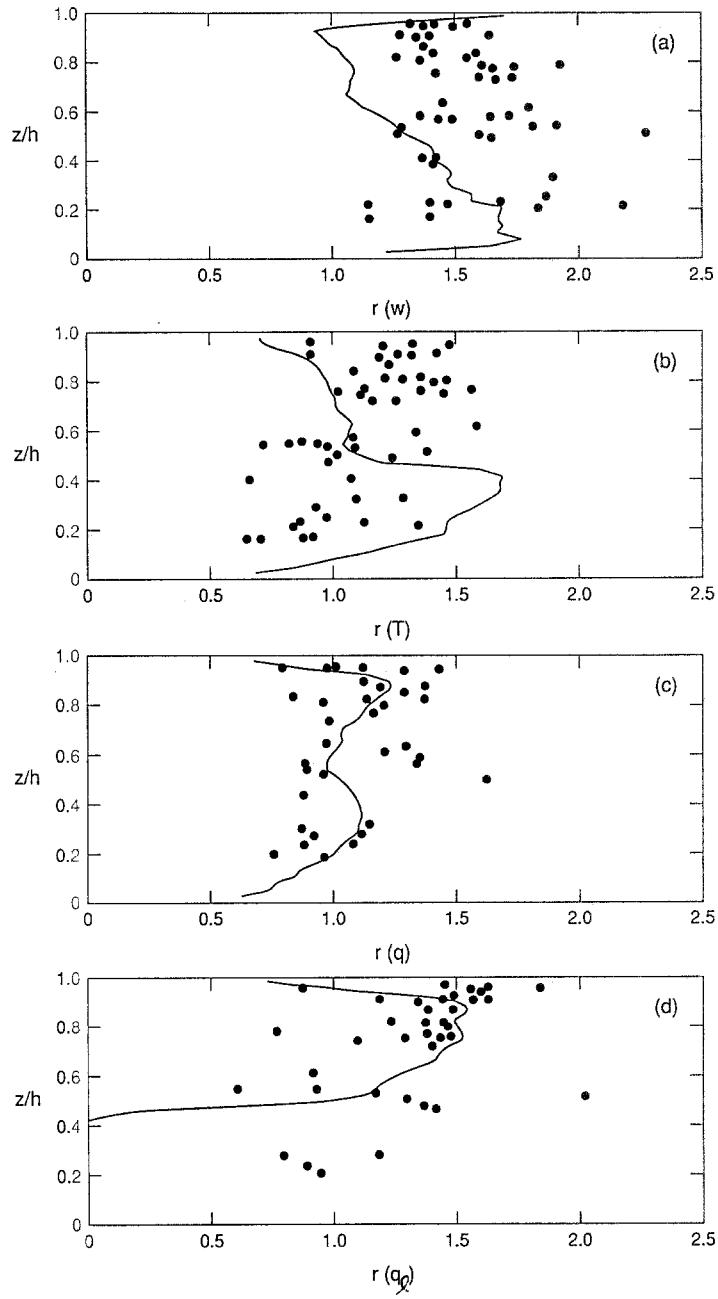

Fig. 13. Comparison of (a) $r(w)$, (b) $r(T)$, (c) $r(q)$, (d) $r(q_l)$ computed from the LES (solid lines) with the measured data (dots).

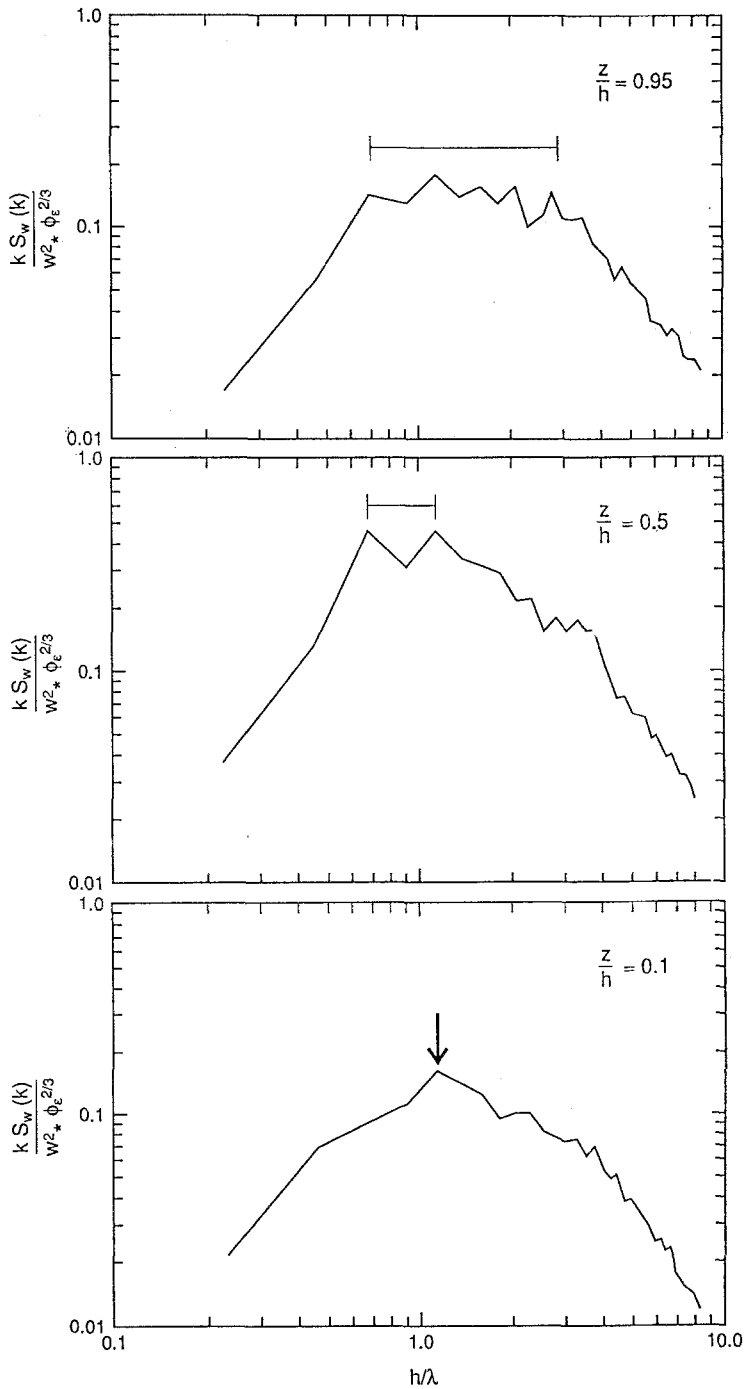

Fig. 14. Normalized vertical velocity spectra as a function of the dimensionless wavelength, h/λ, at three different heights. The bars cover the broad range of the peak wavelengths predicted from the LES.

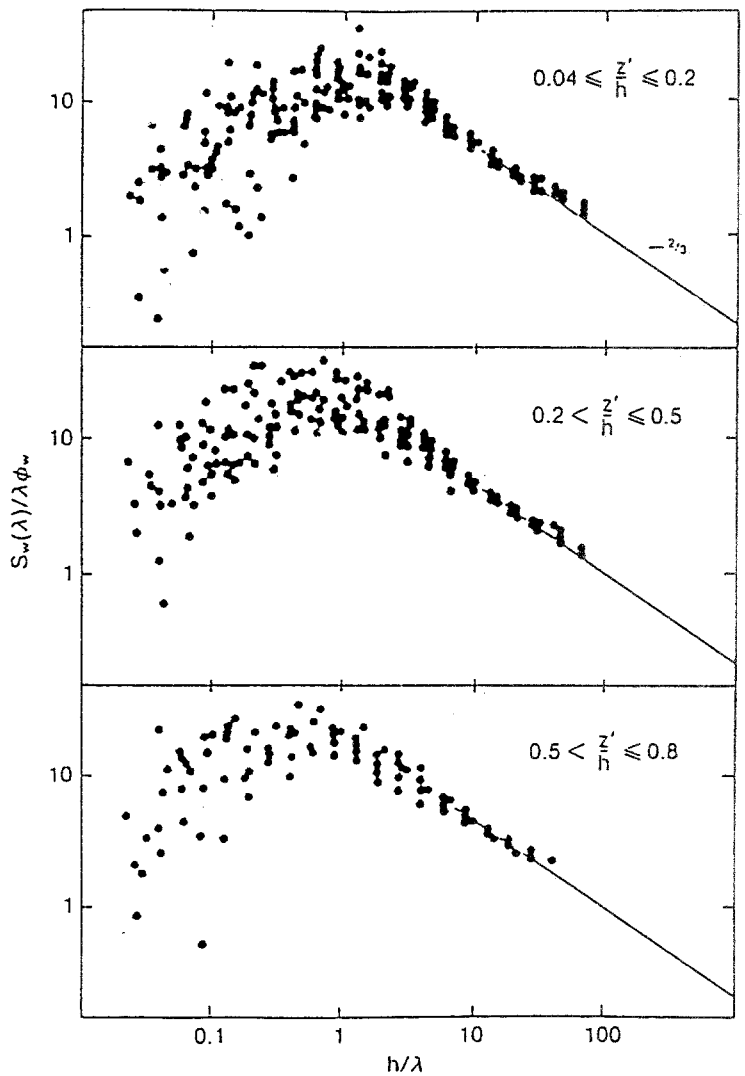

Fig. 15. Same as Figure 14, but from the observations. Note $z'/h = 1 - z/h$. (This figure is taken from Nicholls, 1989.)

by Nucciarone and Young (1991). They analyzed the turbulence spectra in a marine stratocumulus-topped boundary layer using the FIRE data, and found that the spectral peak between $0.1z_i$ and $0.4z_i$ occurs at a scale smaller than that between $0.4z_i$ and $0.9z_i$.

3.6. Turbulent kinetic energy budgets

Nicholls (1989) compared the turbulent kinetic energy budgets of his aircraft data with those obtained from an early stratus LES reported in Moeng (1986). The

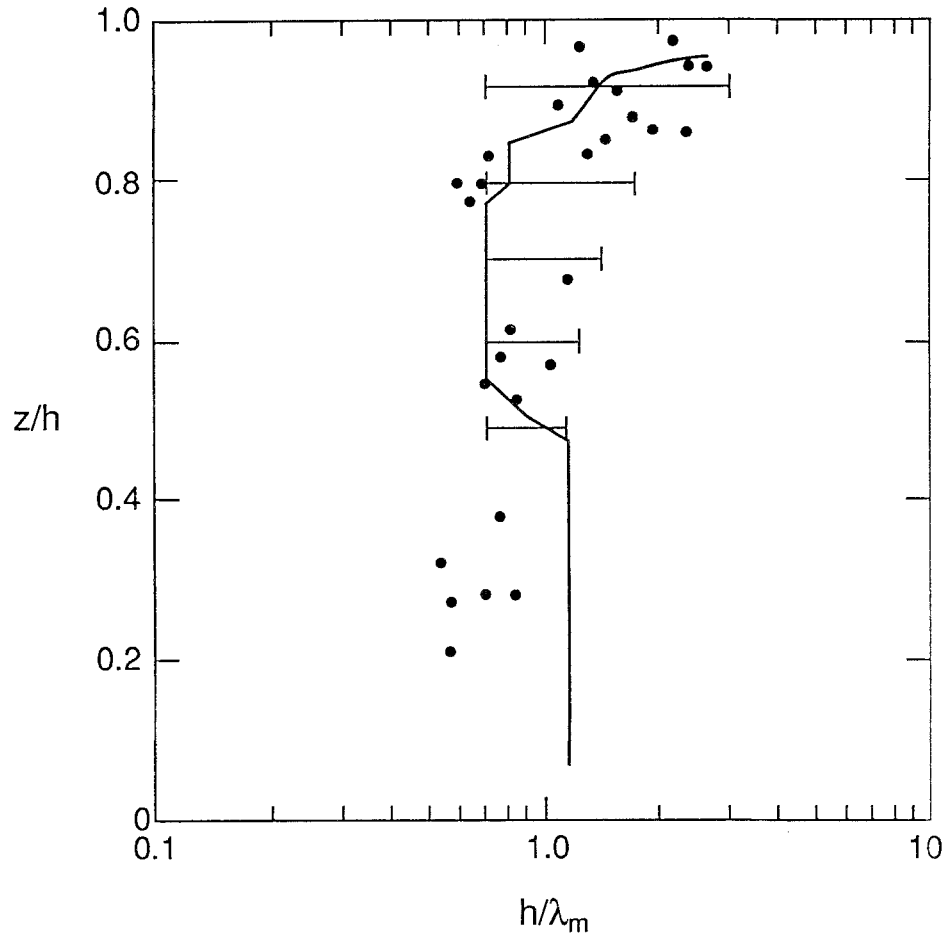

Fig. 16. Vertical distributions of the spectral peak wavelengths, h/λ_m computed from the LES (solid lines with bars) and the measured data (dots). The bars cover the broad range of the peak wavelengths as indicated in Figure 14.

early LES had $40 \times 40 \times 40$ grid points covering a $5 \times 5 \times 2$ km numerical domain; hence it had a horizontal resolution that was ten times coarser than the LES reported here. In this paper, we compare the TKE budgets of the fine LES with those of Nicholls, in Figure 17. We observe some similarities. Close to the cloud top, i.e., above $z/h \sim 0.9$, the pressure transport is a major source. Only where $z/h \sim 0.85$, does the buoyancy term become a major energy source. The positive buoyancy term is due to the fact that most of the cloud-top radiative cooling is incorporated into downdrafts. The turbulent transport term (T-term, i.e., the convergence of the third moment $\overline{wE}$, where E is the turbulent kinetic energy) and the pressure transport term (which is denoted as P in the LES and I in

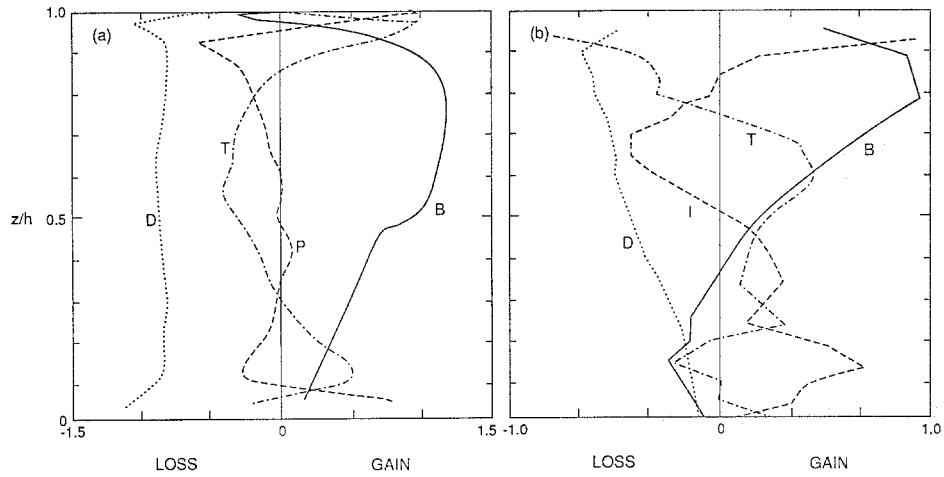

Fig. 17. Budgets of the turbulent kinetic energy from (a) the LES and (b) the measured data (taken from Nicholls, 1989). The mean-shear production term (not shown) from the LES is negligibly small except very close to the surface.

Nicholls' results) tend to cancel one another. This leads to a near balance between the buoyancy and dissipation terms in most of the mixed layer.

However, there is a major discrepancy. The vertical distribution of T throughout the PBL in the LES is almost opposite to that in Nicholls' observations. Near the cloud top, above $0.8h$, the simulated T-term is a source while the observed T is a large sink. In the middle of the mixed layer, the simulated T becomes a sink while the observed T becomes a source. This discrepancy was also pointed out by Nicholls in an early comparison with Moeng's $(40)^3$ LES.

To examine this major discrepancy, we show the vertical transport of the turbulent kinetic energy from LES, $\overline{wE}$, in Figure 18. The LES profile is totally different from the observations of Nicholls (1989). We also show $\overline{w^3}$ from our LES in Figure 18, and find that it is responsible for almost all of the total energy transport. Therefore, the major discrepancy between observations and our LES is mainly in the $\overline{w^3}$ field, also pointed out by Nicholls. The measurements indicated large negative $\overline{w^3}$ in the upper layer, where LES indicates positive $\overline{w^3}$.

This puzzle was studied by Moeng and Rotunno (1990); they examined the vertical velocity skewness $\overline{w^3}/\overline{w^2}^{(3/2)}$ using direct numerical simulations of medium Reynolds number convection within two parallel plates. They found that when the parallel plate convection is heated from below and cooled from above, the vertical velocity skewness is positive in the upper part and negative in the lower part. This seems contradictory to one's intuition that the bottom heating should generate a positive skewness in the lower layer and the top cooling should generate a negative skewness in the upper layer. Moeng and Rotunno showed that the surface-heating-generated updrafts that reach the top of the mixed layer are re-

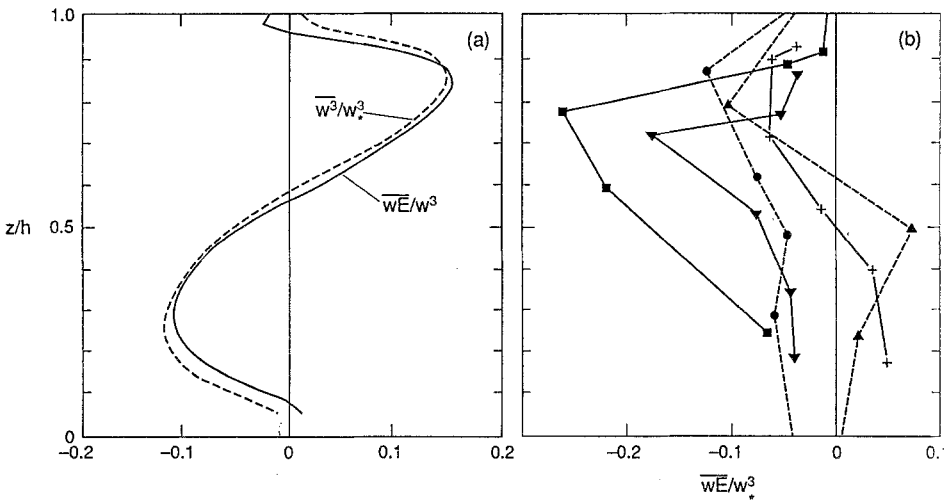

Fig. 18. Vertical profiles of (a) $\overline{wE}$ (solid line) and $\overline{w^3}$ (dash line) from the LES, and (b) $\overline{wE}$ from the measured data (taken from Nicholls, 1989) where five symbols represent the five flight cases.

sponsible for the positive w-skewness in the upper layer, and the top-cooling generated downdrafts that reach the surface are responsible for the negative w-skewness in the lower layer. Their study was able to explain the vertical distribution of the w-skewness (hence of the $\overline{w^3}$) found in LES results; however it does not solve the discrepancy between LES and observations. Nevertheless, they pointed out that when the cloud layer is decoupled from the subcloud layer, the surface-heating-generated updrafts cannot reach the cloud top and therefore the w-skewness profile is changed.

4. Summary and Conclusions

Results have been presented of a large-eddy simulation of the nocturnal stratus-topped boundary layer that has a much finer resolution than previously reported. The simulation is used to assess the realism of large-eddy simulation of the stratus-topped PBL by comparing LES results with aircraft measurements reported by Nicholls (1989).

First we described the basic flow structure of the stratus-topped PBL by examining the instantaneous turbulent field. We showed that the convective motions driven mainly by cloud-top radiative cooling are consistent with the observations. Near cloud top, there are many closed cellular patterns in which updrafts occupied the broad centers and relatively strong downdrafts occurred in a narrow region at the cell edges. Weaker downdrafts that are relatively colder and drier and that occupy the intersections of the cell boundaries are likely to become stronger

downdrafts after descending for some distance below cloud top, with some of them extending all the way to the surface, as observed from Figures 1–4.

We then studied the coherent downdrafts and their small-scale features by using a conditional sampling method similar to that used by Nicholls (1989), and compared the results with Nicholls' measurements. We found that the LES results agree with observations in the upper mixed layer but differences exist in the lower half of the mixed layer. Most of the differences in the lower half, however, can be explained by the decoupling that exists in observations but not in the LES. Our results indicate that the LES of the stratus-topped boundary layer with ~10 m resolution in all three dimensions can resolve most of the observed features.

The peaks of the vertical velocity spectra from the LES become broader and shift to higher wavenumbers with height. These results are in general agreement with those reported by Nicholls (1989). However, in the lower part of the mixed layer, the spectral peaks from the LES have larger wavenumbers than the measurements. This discrepancy may be due to the fact that our lower mixed layer is closer to the rigid surface, because there is no decoupling in our simulated case.

We also compared the TKE budgets and showed that a major discrepancy between LES and observations in the TKE transport term still exists even with a finer-resolution LES. This discrepancy is due to the different behavior in $\overline{w^3}$ between simulations and observations (Moeng and Rotunno, 1990). The physical processes responsible for this difference remain undetermined, but may be associated with decoupling.

Acknowledgments

We thank Steve Krueger, Don Lenschow, Ilga Paluch, Dave Randall, Steve Siems, Steve Stage, Qing Wang, and George Young for helpful reviews, and Hope Hamilton for her careful editing. This work was partially supported by the Office of Naval Research under Interagency Agreement (IA) No. 89-12.

References

Brost, R. A., Lenschow, D. H., and Wyngaard, J. C.: 1982a, 'Marine Stratocumulus Layer. Part I: Mean Conditions', *J. Atmos. Sci.* **3**, 800–817.

Brost, R. A., Wyngaard, J. C., and Lenschow, D. H.: 1982b, 'Marine Stratocumulus Layer. Part II: Turbulence Budgets', *J. Atmos. Sci.* **3**, 818–836.

Caughey, S. J., Crease, B. A., and Roach, W. T.: 1982, 'A Field Study of Nocturnal Stratocumulus. II: Turbulence Structure and Entrainment', *Quart. J. Roy. Meteorol. Soc.* **108**, 125–144.

Clark, T. L.: 1979, 'Numerical Simulations with a Three-Dimensional Cloud Model: Lateral Boundary Condition Experimenta and Multicellular Severe Storm Stimulations', *J. Atmos. Sci.* **36**, 2191–2215.

Deardorff, J. W.: 1974, 'Three-Dimensional Numerical Study of Turbulence in an Entraining Mixed Layer', *Boundary-Layer Meteorol.* **7**, 199–226.

Deardorff, J. W.: 1980a, 'Stratocumulus-Capped Mixed Layers Derived from a Three-Dimensional Model', *Boundary-Layer Meteorol.* **18**, 495–527.

Deardorff, J. W.: 1980b, 'Cloud-Top Entrainment Instability', *J. Atmos. Sci.* **37**, 131–147.

Kaimal, J. C., Wyngaard, J. C., Haugen, D. A., Coté, O. R., Izumi, Y., Caughey, S. J.,and Readings,

C. J.: 1976, 'Turbulence Structure in the Convective Boundary Layer', *J. Atmos. Sci.* **33**, 2152–2169.

Khalsa, S. J. S. and Greenhut, G. K.: 1985, 'Conditional Sampling of Updrafts and Downdrafts in the Marine Atmospheric Boundary Layer', *J. Atmos. Sci.* **42**, 2550–2562.

Lenschow, D. H. and Stephens, P.: 1980, 'The Role of Thermals in the Convective Boundary Layer', *Boundary-Layer Meteorol.* **19**, 509–531.

Mason, P. J.: 1989, 'Large-Eddy Simulation of the Convective Atmospheric Boundary Layer', *J. Atmos. Sci.* **4**, 1192–1516.

Moeng, C.-H.: 1984, 'A Large-Eddy-Simulation Model for the Study of Planetary Boundary-Layer Turbulence', *J. Atmos. Sci.* **41**, 2052–2062.

Moeng, C.-H.: 1986, 'Large-Eddy Simulation of a Stratus-Topped Boundary Layer. Part I: Structure and Budgets', *J. Atmos. Sci.* **43**, 2886–2900.

Moeng, C.-H. and Schumann, U.: 1991, 'Composite Structure of Plumes in Stratus-Topped Boundary Layers', *J. Atmos. Sci.* **48**, 2280–2291.

Moeng, C.-H. and Rotunno, R.: 1990, 'Vertical-Velocity Skewness in the Buoyancy Driven Boundary Layer', *J. Atmos. Sci.* **47**, 1149–1162.

Moeng, C.-H. and Wyngaard, J. C.: 1984, 'Statistics of Conservative Scalars in the Convective Boundary Layer', *J. Atmos. Sci.* **41**, 3161–3169.

Moeng, C.-H. and Wyngaard, J. C.: 1986, 'An Analysis of Closures for Pressure-Scalar Covariances in the Convective Boundary Layer', *J. Atmos. Sci.* **43**, 2499–2513.

Moeng, C. and Wyngaard, J. C.: 1989, 'Evaluation of Turbulent Transport and Dissipation Closures in Second-Order Modeling', *J. Atmos. Sci.* **46**, 2311–2330.

Nicholls, S.: 1984, 'The Dynamics of Stratocumulus: Aircraft Observations and Comparisons with a Mixed Layer Model', *Quart. J. Roy. Meteorol. Soc.* **110**, 783–820.

Nicholls, S.: 1989, 'The Structure of Radiatively Driven Convection in Stratocumulus', *Quart. J. Roy. Meteorol. Soc.* **115**, 487–511.

Nicholls, S. and Leighton, J. R.: 1986, 'An Observational Study of the Structure of Stratiform Cloud Sheets. Part 1. Mean Structure', *Quart. J. Roy. Meteorol. Soc.* **112**, 431–460.

Nicholls, S. and Readings, C. J.: 1981, 'Spectral Characteristics of Surface Layer Turbulence Over the Sea', *Quart. J. Roy. Meteorol. Soc.* **107**, 591–614.

Nicholls, S. and Turton, J. D.: 1986, 'An Observational Study of the Structure of Stratiform Cloud Sheets. Part: Entrainment', *Quart. J. Roy. Meteorol. Soc.* **112**, 461–480.

Nucciarone, J. J. and Young, G. S.: 1991, 'Aircraft Measurements of Turbulence Spectra in the Marine Stratocumulus-Topped Boundary Layer', *J. Atmos. Sci.* **48**, 2382–2392.

Randall, D. A.: 1980, 'Conditional Instability of the First Kind Upside-Down', *J. Atmos. Sci.* **37**, 125–130.

Schmidt, H. and Schumann, U.: 1989, 'Coherent Structure of the Convective Boundary Layer Derived from Large-Eddy Simulations', *J. Fluid Mech.* **200**, 511–562.

Schumann, U. and Moeng, C.-H.: 1991a, 'Plume Fluxes in Clear and Cloudy Convective Boundary Layers', *J. Atmos. Sci.* **48**, 1746–1757.

Schumann, U. and Moeng, C.-H.: 1991b, 'Plume Budgets in Clear and Cloudy Convective Boundary Layers', *J. Atmos. Sci.* **48**, 1758–1770.

Slingo, A., Brown, R., and Wrench, C. L.: 1982, 'A Field Study of Nocturnal Stratocumulus III. High Resolution Radiative and Microphysical Observations', *Quart. J. Roy. Meteorol. Soc.* **108**, 145–165.

Young, G. S.: 1988a, 'Turbulence Structure of the Convective Boundary Layer. II: Phoenix 78 Aircraft Observations of Thermals and their Environment', *J. Atmos. Sci.* **45**, 727–735.

Young, G. S.: 1988b, 'Turbulence Structure of the Convective Boundary Layer. III: The Vertical Velocity Budgets of Thermals and their Environment', *J. Atmos. Sci.* **45**, 2039–2049.